Materials Today Bio 32 (2025) 101788

Contents lists available at ScienceDirect

Materials Today Bio

journal homepage: www.journals.elsevier.com/materials-today-bio

Biocompatible cloaking of bacteria for effective tumor imaging and therapy

Qing Guan [a], Junjie Chen [a], Zhaonan Liu [a], Jianfeng Xin [a], Yu Chen [a], Peng Wang [a], Jun Liu [a,b,*]

[a] Key Laboratory of Marine Drugs, Ministry of Education, School of Medicine and Pharmacy, Ocean University of China, Qingdao, 266003, China
[b] Laboratory for Marine Drugs and Bioproducts, Qingdao Marine Science and Technology Center, Qingdao, 266237, China

ARTICLE INFO

Keywords:
Bacteria
Biomaterials coating
Biocompatibility
Tumor imaging
Tumor therapy

ABSTRACT

Bacteria possess distinctive characteristics, such as tropism, motility, and genetic editability, which make them highly attractive for biomedical applications, such as tumor imaging and therapy. However, the immunogenicity triggered by endotoxins may lead to severe adverse effects and prompt quick elimination in the body, thus restricting their clinical applications. In this study, we described a double-layer coating technique employing tannic acid (TA) and albumin (BSA) for bacteria encapsulation. This compact coating effectively shields endotoxin exposure and inhibits endotoxin leakage from bacteria, exhibiting a favorable safety profile. Moreover, bacteria coated with BSA have superior biocompatibility with their surroundings, which prevents phagocytes from eliminating the bacteria, hence prolonging the reservation in vivo. As bacteria grow, the BSA-TA layer progressively detaches after reaching targeted sites, allowing free bacteria to exploit their own advantages. Importantly, the BSA-TA coating strategy protects bacteria against various environmental assaults without compromising their growth, proliferation, or motility, maintaining their inherent characteristics. In murine tumor models, the BSA-TA-coated bacteria demonstrated enhanced long-term tumor imaging and therapeutic efficacy against tumors. Together, the BSA-TA coating strategy improves the biocompatibility of bacteria and has the capacity to expand the range of bacteria for biomedical applications.

1. Introduction

Bacteria, one of the most abundant species of microorganisms, play a critical role in maintaining the immune and metabolic homeostasis of the human body [1,2]. They possess a variety of unique characteristics that make them well-suited for multiple biomedical applications [3,4]. Due to their ability to regulate the balance of the gut microbiota, bacteriotherapy is commonly used to treat infectious diseases in the gastrointestinal (GI) tract, such as fecal microbiota transplantation for drug-refractory *Clostridium difficile* infection [5]. Additionally, the numerous features of bacteria, such as tropism and motility, provide them with many potential purposes [6,7]. For instance, bacteria may be used as an intelligent drug delivery platform due to their tropism for hypoxic microenvironments, light, or external magnetic fields, which effectively orients them to recognize and respond to various stimuli in the surroundings [8,9]. Moreover, the motility driven by rotating flagella and pili facilitates the bacteria to move and colonize in targeted positions [10,11]. Due to the immunosuppressive nature of the tumor microenvironment (e.g., the enrichment of myeloid-derived suppressor cells and regulatory T cells) [12], bacteria preferentially target and colonize tumor sites, allowing them to evade immune clearance [13]. Moreover, the hypoxic regions within solid tumors provide a selective growth advantage for anaerobic or facultative anaerobic bacteria [14], resulting in colonization efficiency up to 1000 times higher than in normal tissues [15]. Consequently, bacteria can effectively target tumor tissues for tumor imaging and therapy. In addition to these purposes, bacteria are also used in vaccine development and diagnosis [16–18].

In spite of the numerous advantages of bacteria for biomedical uses, its widespread application is dampened by its low efficiency and unavoidable side effects caused by immunogenicity [19,20]. Specifically, bacteria are easily recognized and cleared by phagocytes before colonizing targeted sites, resulting in limited reservation in vivo and reduced treatment efficacy [21]. Furthermore, the presence of endotoxins in the bacterial wall may lead to serious adverse effects, such as cytokine storm, fever, and even septic shock [22,23]. Knocking out virulence genes for detoxification may effectively decrease endotoxin levels [24,25]. However, that will result in the irreversible loss of the immunogenicity of bacteria to stimulate an immune response in the host, which

* Corresponding author. Key Laboratory of Marine Drugs, Ministry of Education, School of Medicine and Pharmacy, Ocean University of China, Qingdao, 266003, China.
E-mail address: jliu1102@ouc.edu.cn (J. Liu).

https://doi.org/10.1016/j.mtbio.2025.101788
Received 20 February 2025; Received in revised form 8 April 2025; Accepted 21 April 2025
Available online 22 April 2025

is important for disease treatment, such as tumor immunotherapy [26,27]. Therefore, there remains an urgent need to develop innovative methods to improve the biocompatibility of bacteria to ensure safe and effective applications, while preserving their inherent properties.

In this study, we developed a BSA-TA coating strategy for bacteria encapsulation that significantly enhanced bacterial biocompatibility and increased the reservation duration of bacteria in vivo (Fig. 1). Firstly, to avoid the exposure of endotoxins on bacterial surfaces, we chose TA, a compound having a similar structure to the components of mussel adhesive *Mytilus edulis* foot proteins and possessing a strong adhesive capacity [28,29], to encapsulate bacteria. The TA molecule could immediately form a compact layer on the surface of bacteria via crosslinking with ferric ions. Apart from shielding endotoxins from exposure, the compact TA layer might also impede the penetration of macromolecules, including endotoxins, while permitting small molecules diffusion to ensure bacterial growth and proliferation. Additionally, to improve bacterial biocompatibility, the TA-encapsulated bacteria was further coated with albumin (BSA), a protein commonly present in blood. This BSA layer affords bacteria good compatibility with living organisms and camouflages bacteria from being phagocytized by phagocytes, therefore extending the reservation of bacteria in vivo. Moreover, after the BSA-TA coating, bacteria exhibited a favorable safety profile and would not cause any stress responses, even when administered intravenously. In addition, the BSA-TA layer provides protection for bacteria against various environmental invasions, which is beneficial for bacteria storage and transportation. Importantly, the natural properties of bacteria are preserved, given that the BSA-TA coating has no influence on bacteria growth and proliferation, as well as their motility. Notably, the BSA-TA coating is stable while bacteria are inactive, but it gradually detaches when bacteria grow and release free bacteria, allowing them to exploit their natural benefits. Furthermore, by establishing tumor-bearing mice models, we demonstrated that BSA-TA-encapsulated bacteria markedly improved long-term tumor imaging and exhibited robust anti-tumor efficacy. Collectively, we developed a simple and scalable BSA-TA coating strategy, which provides bacteria with high biocompatibility and has the potential to broaden the biomedical applications of bacteria in tumor imaging and therapy.

2. Materials and methods

2.1. Materials

The chemicals and biologicals used in this study were listed as follows: Tannic acid (TA, Heowns), Iron(III) chloride hexahydrate ($FeCl_36H_2O$, Macklin), 3-(N-morpholino) propane sulfonic acid (MOPS, Bidepharm), Bovine Serum Albumin (BSA, Yeasen), Calcium chloride ($CaCl_2$, Yuanye), Sodium alginate (200 ± 20mpa.s, Aladdin), Ampicillin (Bidepharm), Lysozyme (Bidepharm), Hydrogen peroxide solution (H_2O_2, Macklin), Sodium chloride (NaCl, Fangzheng), Rhodamine B-NHS (Sigma), FITC (Aladdin), FITC-PEG (Yusiyy), Cell counting kit-8 (CCK-8, Beyotime), Mice inflammatory factor ELISA kit (Pepro Tech), Endotoxin detection kit (Beyotime), and Triton X-100 (Biotopped). The Luria-Bertani (LB, Hopebio) liquid medium was prepared by dissolving 25 g of LB broth in 1 L of deionized (DI) water and sterilized by autoclave. LB agar plates were prepared on dishes with 15 mL of LB agar solution (containing 25 g of LB broth and 15 g of agar in 1 L of DI water).

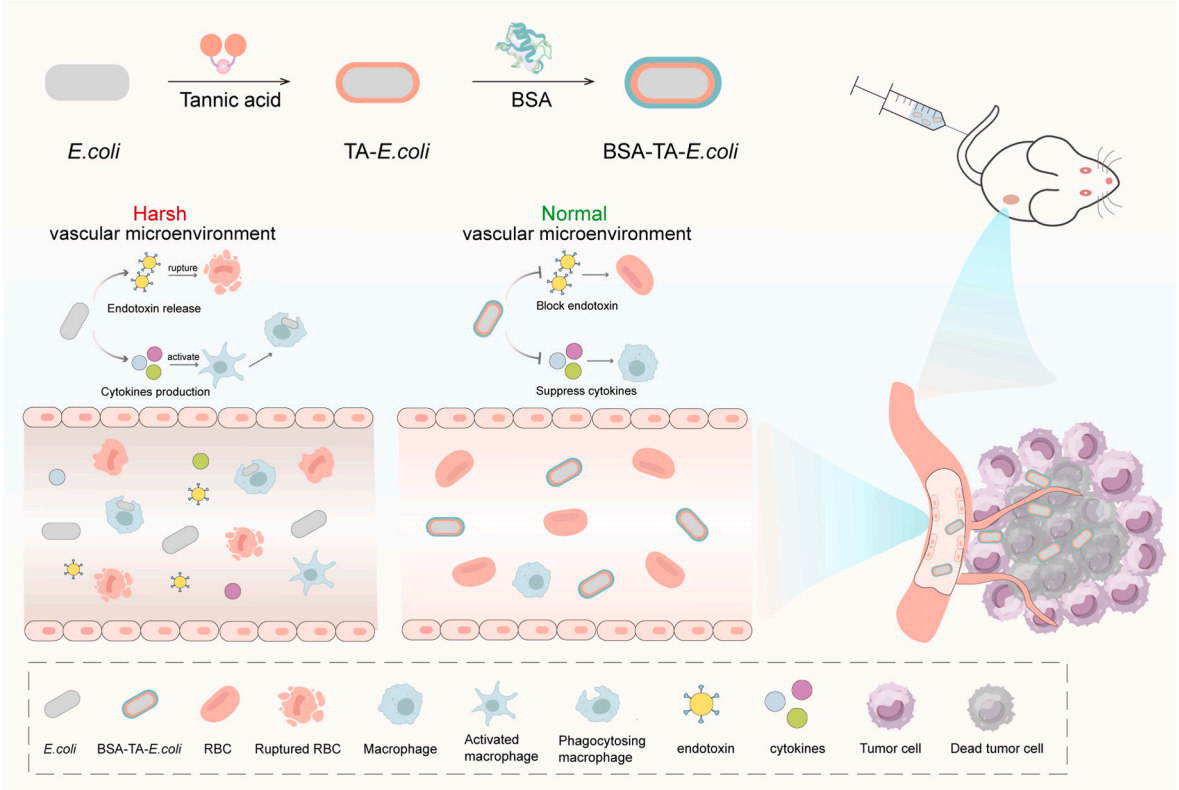

Fig. 1. Schematic illustration of preparing BSA-TA-encapsulated bacteria that showed improved biocompatibility, enhanced tumor targeting and imaging, and potent anti-tumor efficacy in vivo. The immunogenicity of bacteria would cause acute stress responses and result in severe side effects, such as hemolysis, which impede the application of bacteria in biomedical areas. The formed compact BSA-TA layer could prevent the exposure and leakage of endotoxins, and shield bacteria from their surroundings, exhibiting excellent biocompatibility. Importantly, the BSA-TA layer would not affect the growth, proliferation, and motility of bacteria, preserving their natural characteristics. The BSA-TA coating strategy has the capacity to broaden the range of bacteria in biomedical applications, such as tumor imaging and bacteriotherapy against tumors.

2.2. Methods

2.2.1. Strains and cultural conditions

The *Escherichia coli* (*E.coli*), *Escherichia coli* Nissle (EcN), and Lactobacillus rhamnosus GG (LGG) strains were used in this study. The *E.coli* and EcN cells were cultured on an LB agar plate, while the LGG cells were cultured on a Mars agar plate. Prior to each experiment, the cells were incubated in liquid media overnight at a shaking speed of 220 rpm at 37 °C.

2.2.2. Encapsulation of E.coli with TA

After being removed from an LB agar plate, the *E.coli* cells were grown in liquid LB medium overnight at 37 °C. Subsequently, the *E.coli* cells were resuspended in 490 μL of DI water after being washed twice with DI water. Next, TA solution (5 μL, 40 mg/mL) and $FeCl_3$ solution (5 μL, 10 mg/mL) were successively added to the suspension, and the resulted mixture was gently vortexed for 20 s. After that, the pH was stabilized by adding 0.5 mL of MOPS buffer (20 mM, pH 7.4) to the mixture, leading to the formation of a stable TA layer on the *E.coli* surface. After being washed with DI water twice to remove residual TA and $FeCl_3$, the formed TA-*E.coli* cells were collected by centrifugation.

2.2.3. Encapsulation of TA-E.coli with BSA

The formed TA-*E.coli* cells were resuspended in 990 μL of DI water, 10 μL of BSA solution (40 mg/mL) was added to the suspension, and the mixture was incubated for 30 min at a shaking speed of 220 rpm at room temperature. After that, the formed BSA-TA-*E.coli* cells were collected by centrifugation after being washed with DI water twice to remove residual BSA.

2.2.4. Characterization of E.coli, TA-E.coli, and BSA-TA-E.coli

The morphologies of *E.coli* and TA-*E.coli* were visualized by scanning electron microscopy (SEM). Specifically, the bacteria samples were fixed with 2.5 % glutaraldehyde for 4h at 4 °C. After aspirating the fixative, the samples were rinsed 3 to 5 times, and then dehydrated with a series of gradient concentrations of ethanol (30 %, 50 %, 70 %, 80 %, 90 %, 95 %, and 100 %) for 15 min each. After drying completely, the samples were observed and imaged under SEM. In addition, the morphologies of *E.coli*, TA-*E.coli*, and BSA-TA-*E.coli* were further visualized via transmission electron microscopy (TEM, JEM-1200EX). Briefly, a droplet of bacterial solution was deposited onto a carbon-coated copper grid. Then, the samples were washed with DI water, dried completely in the air, and photographed by TEM. Moreover, the encapsulation of *E.coli* in the BSA layer was also characterized by laser scanning confocal microscopy (LSCM). Briefly, TA-*E.coli* was mixed with Rhodamine B-labeled BSA solution and incubated for 30 min to prepare Rhodamine B-labeled BSA-TA-*E.coli*, which was then subjected to LSCM for observation and imaging. Furthermore, the particle sizes and zeta potentials of *E.coli*, TA-*E.coli*, and BSA-TA-*E.coli* were determined by dynamic light scattering (DLS).

2.2.5. Measurement of growth curves of E.coli, TA-E.coli, and BSA-TA-E.coli

The different bacteria formulations were diluted and placed into a 96-well plate with an initial OD_{600} value of ~0.1. The plate was incubated at 37 °C with gentle shaking, and the OD_{600} values were monitored using a microplate reader (HBS-Scan Y, DeTie) for 12 h at intervals of 0.5 h. Uncoated *E.coli* served as a control.

2.2.6. Cell viability assay

Using a cell counting kit-8 (CCK-8), cell viability was examined in accordance with the manufacturer's instructions. Briefly, 100 μL of LB medium containing *E.coli*, TA-*E.coli*, and BSA-TA-*E.coli* were individually seeded into a 96-well plate, with an initial OD_{600} value of around 0.15. Afterward, CCK-8 solution (10 μL) was added into each well and incubated at 37 °C. A microplate reader was applied to record the OD_{450} values for 4 h, at 1-h intervals.

2.2.7. Bacteria tropism assay

The bacteria tropism after the BSA-TA coating was evaluated using a transwell migration assay. Briefly, bacteria were suspended in 1 % NaCl solution, and the concentration was adjusted to an OD_{600} value of 0.15. Then, 200 μL of the bacterial solution was added to the upper compartment of a transwell chamber, while the lower compartment contained 700 μL of LB medium. 700 μL of 1 % NaCl solution placed in the lower compartment served as a control. At predetermined time points of 10 min, 30 min, 1 h, and 2 h, the solutions in the lower compartment were taken and spread on LB agar plates after gradient dilutions. The colonies were counted after the LB agar plates grew for 24 h at 37 °C.

2.2.8. Resistance assay

1×10^8 CFU of *E.coli* and BSA-TA-*E.coli* cells were subjected to LB media containing 0.25 mg/mL of ampicillin, 20 mg/mL of lysozyme, or hydrogen peroxide (80 mM), respectively. At predetermined time points, 50 μL of each sample was taken, washed with DI water, and spread on LB agar plates in sequential 10-fold dilutions. The colonies were counted after 24 h of incubation at 37 °C. For ultraviolet (UV) resistance, *E.coli* and BSA-TA-*E.coli* cells were placed in LB media and cultured under UV light irradiation (254 nm). The bacterial colonies after UV exposure were counted and recorded.

2.2.9. Hemolytic toxicity assay

Whole blood samples were taken from KM mice aged 6–8 weeks. The animal studies were approved by the Institutional Animal Care and Use Committee at the Ocean University of China. Murine red blood cells (RBCs) were separated by centrifugation of the whole blood sample at 200 g for 10 min and washed three times with PBS. 100 μL of the collected RBCs were placed into a 96-well plate and mixed with *E.coli* and BSA-TA-*E.coli* (5×10^5 CFUs), respectively. After incubation at 37 °C for 1 h, the plate was centrifugated at 200 g for 15 min. The supernatant was collected, and the absorbance was measured at 450 nm via a microplate reader. PBS treatment was used as a negative control, and 1 % of the Triton X-100 solution served as a positive control. The following formula was used to calculate the hemolysis percentage: % hemolysis = [(absorbance of samples) – (absorbance of PBS group)] × 100/[(absorbance of Triton X-100 group) - (absorbance of PBS group)].

2.2.10. Mice mortality evaluation

All the animal studies strictly followed the protocols approved by the Institutional Animal Care and Use Committee at the Ocean University of China. After treatment with different bacteria formulations, mice mortality was evaluated by intravenous injection of 100 μL of 1×10^7 CFU of bacterial suspensions of *E.coli* and BSA-TA-*E.coli* (n = 6). The mice's survival was recorded in the following days. PBS treatment served as the negative control.

2.2.11. Endotoxin assay

The endotoxin levels after *E.coli* and BSA-TA-*E.coli* treatment were assessed via an endotoxin detection kit (Beyotime, China) according to the manufacturer's instructions. Briefly, 6-8 weeks-old mice were randomly assigned to two groups, with three mice in each group, and the mice were injected with 1×10^7 CFUs of *E.coli* and BSA-TA-*E.coli*, respectively. At predetermined time points, blood was drawn, and the serum was separated by centrifugation at 3000 rpm for 15 min. The 10 μL of serum was placed in a 96-well plate without endotoxins, and mixed with 10 μL of endotoxin detection reagent. The endotoxin detection water served as a negative control. The mixture was incubated in the dark for 15 min at 37 °C. Then, 10 μL of chromogenic reagent solution was added and incubated at 37 °C for an additional 6 min. After that, 50 μL of Buffer A, B, and C were added to each well successively. After resting for 5 min, the absorbance of OD_{545nm} was measured and

recorded using a microplate reader.

2.2.12. Measurement of cytokine levels

Cytokines, including IL-6, IL-10, TNF-α, IFN-γ, and IL-17A, were measured using commercially available ELISA kits (Pepro Tech, USA) according to the manufacturer's instructions. All the methods for detecting these cytokines are similar. The description for IL-6 was chosen as an example and provided below. Briefly, Mice blood was drawn after treating *E.coli* or BSA-TA-*E.coli* intravenously for 30 min and 4 h. After resting for 1 h, the blood was centrifugated at 3000 rpm for 15 min to collect the serum for cytokines detection. Firstly, 100 μL of captured antibody was added to an ELISA plate and incubated at room temperature overnight. Then, the captured antibody residue was aspirated out, and the plate wells were washed with wash buffer 4 times. After that, 300 μL of block buffer was added, and the plate was further incubated for 1 h. After washing the plate, 100 μL of standards and the serums were added, respectively, and the sample was incubated for an additional 2 h. Next, the plate wells were washed with wash buffer 4 times, and 100 μL of detection antibody was added and incubated at room temperature for 2 h. Then, the plate wells were washed with wash buffer again 4 times, and 100 μL of Avidin-HRP conjugate was added. After incubation for 30 min at room temperature, 100 μL of ABTS liquid was added. The absorbance of OD_{405} was detected and recorded using a microplate reader.

2.2.13. Complete blood counts

After injecting mice with 1×10^7 CFUs of *E.coli* or BSA-TA-*E.coli* through the tail vein for 30 min, blood was taken and placed in anticoagulant tubes. Then, the complete blood counts were measured using an animal blood analyzer (ProCyte Dx™, USA). PBS treatment was used as a negative control.

2.2.14. Phenol sulfuric acid method for detecting lipopolysaccharide content

A gradient concentration of lipopolysaccharide solution was prepared. Subsequently, 0.1 mL of the solution was mixed with 0.1 mL of 6 % phenol. After that, 0.5 mL of concentrated sulfuric acid was quickly added, shaken well, and kept standing for 30 min. The absorbance at 490 nm was measured, and the standard curve was drawn. The samples were prepared similarly, and the concentration of lipopolysaccharide was calculated based on the standard curve.

2.2.15. Evaluate the reservation time in vivo

To evaluate whether the reservation time of bacteria could be prolonged after the BSA-TA encapsulation, different bacteria formulations with bioluminescence were injected into mice intravenously and imaged by an in vivo imaging system (IVIS, Caliper LifeSciences, USA). Due to the toxicity of *E.coli*, which can lead to mouse death, EcN with lower toxicity was selected for this study. Briefly, 6–8 weeks-old male mice were randomly assigned into two groups ($n = 3$ in each group) and intravenously injected with 1×10^7 CFUs of EcN or BSA-TA-EcN. At predetermined time points, the bioluminescence signals in mice were monitored and imaged by an IVIS.

2.2.16. In vitro macrophage uptake

The shielding effect of the BSA-TA layer against bacterial elimination was evaluated by measuring the phagocytized rate by phagocytes. Here, the Mouse Leukemia Virus-induced Macrophage Cell line (RAW264.7) was used in this study as a model phagocyte. Briefly, 2×10^6 RAW264.7 cells were seeded in a six-well plate, and cultured at 37 °C for 1 h to allow them adhesion. Before adding to the plate, bacteria were labeled with Rhodamine B by mixing Rhodamine B-NHS with bacteria in the dark for 2 h. Then, Rhodamine B-labeled bacteria were encapsulated with TA and BSA. After that, 30 μL of Rhodamine B-labeled *E.coli* and BSA-TA-*E.coli* PBS suspensions were added to the six-well plate containing RAW264.7 cells, and cultured in a CO_2 cell incubator at 37 °C for 1 h. After centrifugation to remove free bacteria, RAW264.7 cells were collected, transferred to a confocal plate, and imaged under fluorescence microscopy. Moreover, the cells phagocytized bacteria were analyzed by flow cytometry for quantification.

2.2.17. Preparation of calcium alginate microspheres

The calcium alginate microspheres were prepared, which mimic bacterial cells and evaluate the penetration capacity of different weight molecules. Briefly, 0.7 % sodium alginate solution was naturally settled into the calcium chloride solution (20 mM) in the form of microdroplets by mechanical spray method. After curing overnight, the prepared calcium alginate microspheres (CAMs) were concentrated by centrifugation at 300*g* for 5 min.

2.2.18. Selective permeability of the BSA-TA layer

To evaluate the permeability of the BSA-TA layer, we prepared CAMs as described above. The CAMs were then encapsulated with TA and BSA layers to form BSA-TA-CAM. After that, BSA-TA-CAMs were mixed with FITC-labeled different-weight molecules, including PEG_{1000}, PEG_{2000}, PEG_{4000}, PEG_{6000}, and free FITC. After co-cultivation of the mixture in DI water for 6 h in the dark, the CAMs were collected by centrifugation at 300*g* for 5 min to remove residue FITC-labeled molecules. Then, the CAMs were transferred to a confocal dish, and the green FITC fluorescence was imaged by fluorescence microscopy to reflect the permeability of the BSA-TA layer to different weight molecules. Uncoated CAMs served as a control.

2.2.19. Evaluating the immunogenicity of E.coli and BSA-TA- E.coli in vitro

To evaluate the immunogenicity of *E.coli* or BSA-TA-*E.coli* in vitro, we set up a transwell assay. The cells of *E.coli* or BSA-TA-*E.coli* in PBS were placed in the upper compartment of a 0.4 μm transwell chamber, while the lower compartment contained immune cells of RAW264.7 or DC2.4 in DMEM medium. After 12 h of indirect co-culture, the cells in the lower chamber were collected and stained with fluorescently labeled antibodies for 15 min. Finally, matured DC2.4 cells (MHC II^{hig_h}) and M1-type macrophages ($F4/80^{hig_h}$ $CD86^{hig_h}$) were detected by flow cytometry.

2.2.20. Stability and detachment of the BSA-TA layer

To study the stability and detachment effect of the BSA-TA layer, BSA was first labeled with Rhodamine B. Briefly, Rhodamine B-NHS was mixed with BSA and stirred for 2 h at room temperature. The Rhodamine B-labeled BSA was purified by dialysis to remove free Rhodamine B. Next, the *E.coli* cells were encapsulated with TA and Rhodamine B-labeled BSA successively to prepare Rhodamine B-labeled BSA-TA-*E.coli*. To test the stability of the BSA-TA layer on the bacterial surface, Rhodamine B-labeled BSA-TA-*E.coli* was suspended in PBS and stored at 4 °C in the dark. At predetermined time points, the fluorescence signal on bacteria was measured by flow cytometry. Additionally, to test the detachment of the BSA-TA layer upon bacteria growth, the Rhodamine B-labeled BSA-TA-*E.coli* was suspended in LB medium and cultured at 37 °C at a shaking speed of 220 rpm. At predetermined time points of 1 h, 2 h, 4 h, 6 h, 8 h, 12 h, and 24 h, the bacteria were taken and washed with PBS twice. Then, the fluorescence of bacteria was observed and imaged by fluorescence microscopy. Moreover, the number of bacteria carrying the BSA layer was quantitatively analyzed by flow cytometry (BD FACSAria II, USA).

2.2.21. Animal models

All procedures complied with all the relevant ethical regulations and followed the protocols approved by the Institutional Animal Care and Use Committee at the Ocean University of China. BALB/c mice (7 weeks old, female) were purchased from Jinan Pengyue Animals Corporation. 4T1 tumor cells were injected subcutaneously (1×10^7 cells per mouse) into the right flanks of BALB/c mice. Upon tumor growth reaching 80–120 mm^3, EcN or BSA-TA-EcN strains with bioluminescence ($1.0 \times$

10^6 cells per mouse) were injected intravenously to evaluate the effectiveness of tumor imaging. At predetermined time points, the bioluminescence signals were imaged via an IVIS. Additionally, for evaluating the therapeutic efficacy against tumors, EcN or BSA-TA-EcN strains (1.0×10^7 cells per mouse) were injected intravenously. Mouse body weight and tumor volume were monitored daily, and tumor volume (V_t) was calculated using the formula: $V_t = 0.5 \times a \times b^2$. In the equation, a and b represent the major and minor diameters of the tumor, respectively.

2.2.22. Statistics

Statistical analysis was evaluated using GraphPad Prism 8. The statistical significance was determined using Student's *t*-test and one-way ANOVA analysis followed by Tukey's or Fisher's LSD multiple comparisons. The differences between experimental and control groups were considered statistically significant at $P < 0.05$. (n.s.) $P > 0.05$, $^*P < 0.05$, $^{**}P < 0.01$, $^{***}P < 0.001$.

3. Results

3.1. Preparation and Characterization of BSA-TA-E.coli

To explore the potential of the BSA-TA layer to shield bacteria from direct contact with their environment and to prevent the release of endotoxins, we chose *E.coli*, a pathogenic strain, as the model bacterium in this study. Firstly, the TA layer was encapsulated on the surface of *E.coli* via sequentially mixing TA and ferric trichloride with *E.coli* for just 10 s either. The phenolic hydroxyl groups on TA would crosslink with ferric ions quickly via the coordinate bond and form a compact layer on the surface of *E.coli*. The TA layer on the bacterial surface was first characterized by scanning electronic microscopy (SEM), shown in Fig. 2A and Fig. S1. The laminated structure was observed on the surface of TA-*E.coli*, while that was smooth for uncoating *E.coli*, suggesting that the bacteria were decorated with the TA layer. Additionally, the element mapping analysis showed increased Fe elements on the TA-*E.coli* surface, compared to that on the surface of *E.coli*, demonstrating the existence of the TA layer on the bacterial surface (Fig. S2). The coated TA layer was further characterized by transmission electron microscopy (TEM), as evidenced by a transparent outer shell on the bacterial surface (Fig. 2B). Moreover, after the process of preparing TA-*E.coli*, the color turned dark blue (Fig. S3), the size of *E.coli* increased from 1364 nm to 1523 nm (Fig. 2C and Fig. S4), and the zeta potential slightly dropped from −31.6 mV to −32.7 mV (Fig. 2D), further confirming the formation of the TA layer on the bacterial surface. Due to the catechol moieties that have a robust capability to form hydrogen bonds, coordinate bonds, and π-π interactions with various substrates, the TA layer on bacterial surface exhibits a strong adhesive property that makes it easier to assemble BSA on the surface by simply mixing ingredients and vortexing for 30 min. According to the SEM and TEM results, more wrinkles exist on the BSA-TA-E.coli surface (Fig. 2A), and a thicker outer layer on BSA-TA-*E.coli* was observed (Fig. 2B), compared to the TA-*E.coli*. Moreover, after BSA encapsulation, the size was increased from 1523 nm to 1827 nm (Fig. 2C and Fig. S4), and the zeta potential was increased from −32.7 mV to −24.7 mV (Fig. 2D) measured by dynamic light scanning (DLS), indicating the formation of the BSA layer on TA-*E.coli*. Furthermore, the existence of the BSA outer shell was confirmed via laser scanning confocal microscopy (LSCM), as evidenced by rhodamine B-labeled BSA wrapped on the surface of TA-*E.coli* (Fig. 2E). Moreover, the encapsulation rate of TA and BSA on bacterial surfaces was investigated. As shown in Fig. 2F and G, the encapsulation rate was related to the bacterial numbers. At a bacterial concentration of 2×10^8 CFUs, the encapsulation rates of TA and BSA were 90 % and 98 %, respectively. Considering the antibacterial potential of TA, we evaluated the effect of different concentrations of TA on bacterial viability. As shown in Fig. 2H, a TA concentration of 0.4 mg/mL used in this study had negligible toxicity to bacteria.

To determine the influence of the preparation method on bacteria, the cell viability was measured after encapsulation of TA and BSA layers. As shown in Fig. 2I, the process of preparing BSA-TA-*E.coli* did not display any toxicity on bacteria measured by a cell counting kit-8 (CCK-8) assay. Moreover, the growth curves of *E.coli*, TA-*E.coli*, and BSA-TA-*E.coli* were monitored for 12 h via OD_{600nm} values (Fig. 2J). The result showed a similar growth rate of bacteria in these groups, demonstrating the negligible influence of BSA and TA coatings on bacterial growth and proliferation. Next, we investigated whether the BSA-TA coating impacts the motion characteristics of bacteria via a transwell migration assay. The *E.coli* and BSA-TA-*E.coli* cells in 1 % NaCl solution were placed on the upper compartment of transwell chambers, respectively, and the LB medium was placed in the bottom (Fig. 2K). At predetermined time points, the LB medium in the bottom compartment was taken and spread on LB agar plates for cell counting. As shown in Fig. 2L and M, and S5, the migrated bacteria to the bottom between *E.coli* and BSA-TA-*E.coli* groups were similar at all times, indicating that the BSA-TA coating would not affect the nutrition-taxis property of bacteria. To verify the universality of this BSA-TA coating for other cells, we expanded this coating strategy to *Escherichia coli* Nissle 1917 (EcN, a gram-negative probiotic) and Lactobacillus rhamnosus GG (LGG, a gram-positive probiotic). As shown in Fig. S6, fluorescence microscopy demonstrated that all the cells were encapsulated with the BSA-TA layer, as evidenced by the presence of rhodamine B-labeled BSA on the surface of the cells. Moreover, the BSA-TA coating had negligible influence on the growth and proliferation of these cells (Fig. S7), indicating the broad application of this coating technique for live cell therapy. Besides BSA, we further verified that the mucoprotein could also adhere on the TA surface, indicating TA's potential for diverse protein adhesion to support different bacterial applications (Fig. S8).

3.2. Protective effects of the BSA-TA layer against environmental assaults on bacteria

Next, we investigated whether the BSA-TA layer could protect bacteria against environmental assaults. Firstly, BSA-TA-*E.coli* was subjected to ampicillin, a model antibiotic usually used for disease treatment. As shown in Fig. 3A, the viability of BSA-TA-*E.coli* was significantly higher than uncoated *E.coli* after incubation with ampicillin for 12, 24, and 36 h, demonstrating that the BSA-TA coating could protect bacteria against antibiotic invasion. That may be attributed to the outer BSA layer, which is composed of various proteins and can bind to the antibiotics, thereby preventing them from reaching the bacterial membrane and disrupting cell wall functions. Additionally, lysozyme, an antimicrobial enzyme, would kill bacteria by hydrolyzing peptidoglycan in bacterial cell walls. Due to the insulating effect of the BSA-TA layer that prevents direct contact between bacteria and lysozyme, BSA-TA-*E.coli* exhibited higher survival rates compared to *E.coli* when exposed to lysozyme for 12, 24, 48, and 72 h (Fig. 3B). Notably, after 72 h, the number of surviving bacteria in the BSA-TA-*E.coli* group was 21 times more than that of uncoated *E.coli*, showing the strong anti-lysozyme impact of the BSA-TA coating. Furthermore, it was found that BSA-TA-*E.coli* showed higher survival rates than *E.coli* in the H_2O_2-containing medium (Fig. 3C). There were still more than 2×10^3 CFUs live bacteria in the BSA-TA-*E.coli* group after 1 h incubation, whereas almost all the uncoated *E.coli* died. This highlights a superior anti-oxidization capability of BSA-TA-*E.coli*, which may be attributed to the phenolic hydroxyl groups on the TA layer. These groups can react with reactive oxygen species to exert antioxidant activity. Additionally, the TA layer exhibits broad-spectrum UV shielding properties, because the Ligand-to-Metal charge transfer system formed between TA and Fe^{3+} could transfer lone pair electrons from the phenolic hydroxyl group to the empty d orbitals of Fe^{3+}, facilitating the absorption of UV light [30]. As a result, the BSA-TA-*E.coli* showed improved tolerance against UV radiation compared to *E.coli*. As shown in Fig. 3D, all the uncoated *E.coli* were dead after 30 min of UV radiation; however, more than 3.7×10^5 CFUs bacteria survived in the BSA-TA-*E.coli* group. Collectively, the BSA-TA

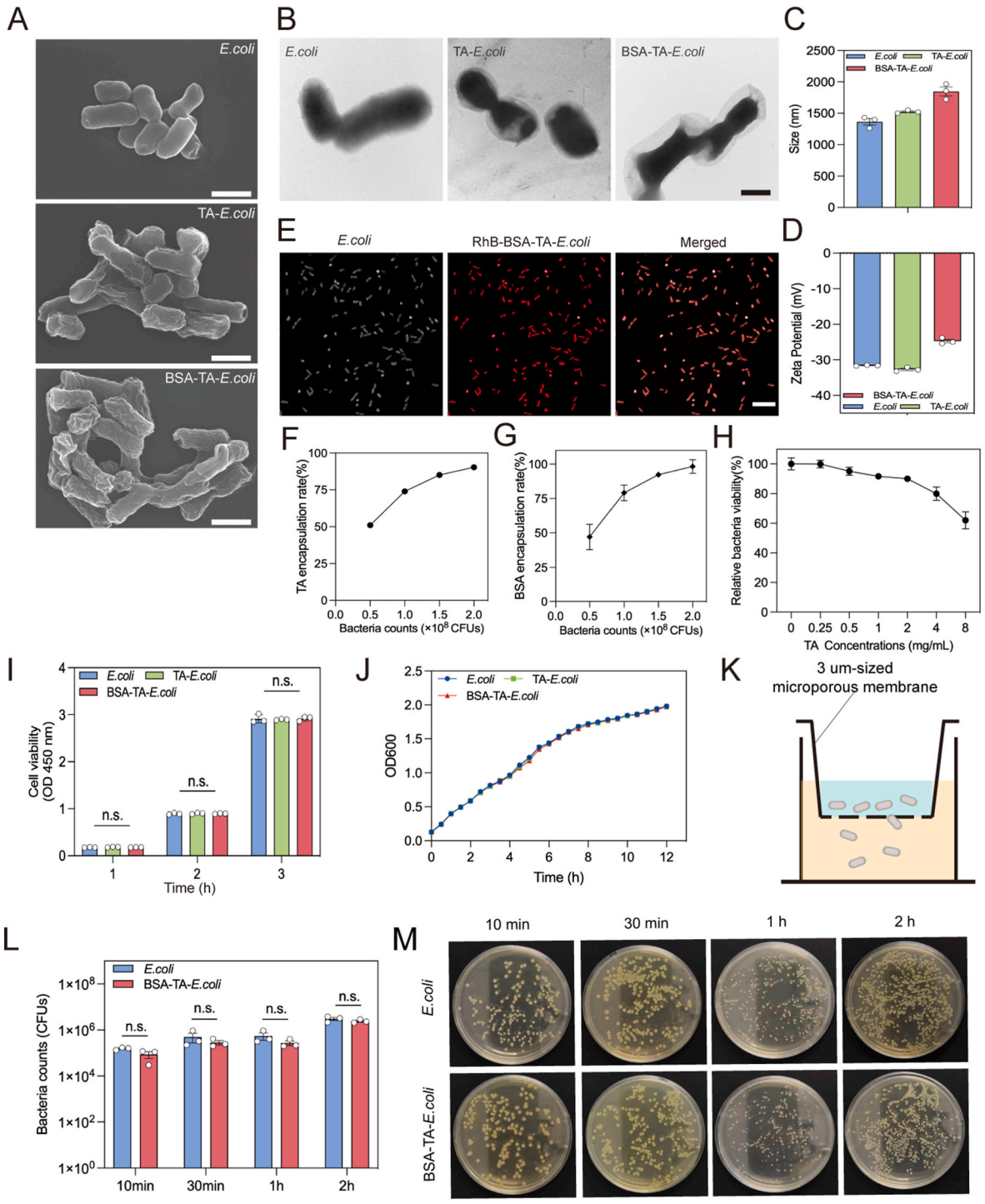

Fig. 2. Preparation and Characterization of BSA-TA-*E.coli*. (**A**) SEM images of *E.coli*, TA-*E.coli* and BSA-TA-*E.coli*. Scale bar, 1 μm. (**B**) TEM images of *E.coli*, TA-*E.coli*, and BSA-TA-*E.coli*. Scale bar, 1 μm. (**C**) Sizes and (**D**) Zeta potentials of *E.coli*, TA-*E.coli*, and BSA-TA-*E.coli* measured by DLS. (**E**) LSCM images of BSA-TA-*E.coli*. The red color represents the BSA layer labeled with Rhodamine B. Scale bar, 20 μm. (**F**) The encapsulation rate of TA on bacteria with different counts. (**G**) The encapsulation rate of BSA on bacteria. (**H**) The toxicity of TA on bacteria detected by a CCK-8 assay. (**I**) Bacteria viability of *E.coli* after encapsulation with the TA layer or both TA and BSA layers analyzed by CCK-8 assay. Non-coated *E.coli* served as the control. Data are presented as means ± SEM ($n = 3$). (**J**) The growth curves of *E.coli*, TA-*E.coli*, and BSA-TA-*E.coli* in LB medium at 37 °C monitored by OD_{600} values in 30-min intervals via a microplate reader. (**K**) Schematic illustration to evaluate the motility characteristics of *E.coli* after BSA-TA coating. (**L**) The nutrient-taxis of *E.coli* and BSA-TA-*E.coli* assessed by transwell migration assay. Bacteria that permeated the transwell membrane at different time points were counted by colony counting. Data are presented as the mean ± SEM ($n = 3$). (**M**) Representative images of bacteria that permeated the transwell membrane at different time points. Statistical analysis was performed using Student's *t*-test for **l** and one-way ANOVA for **c**, **d**, **i**, and **j**. $^{*}P < 0.05$, $^{**}P < 0.01$, $^{***}P < 0.001$. (For interpretation of the references to color in this figure legend, the reader is referred to the Web version of this article.)

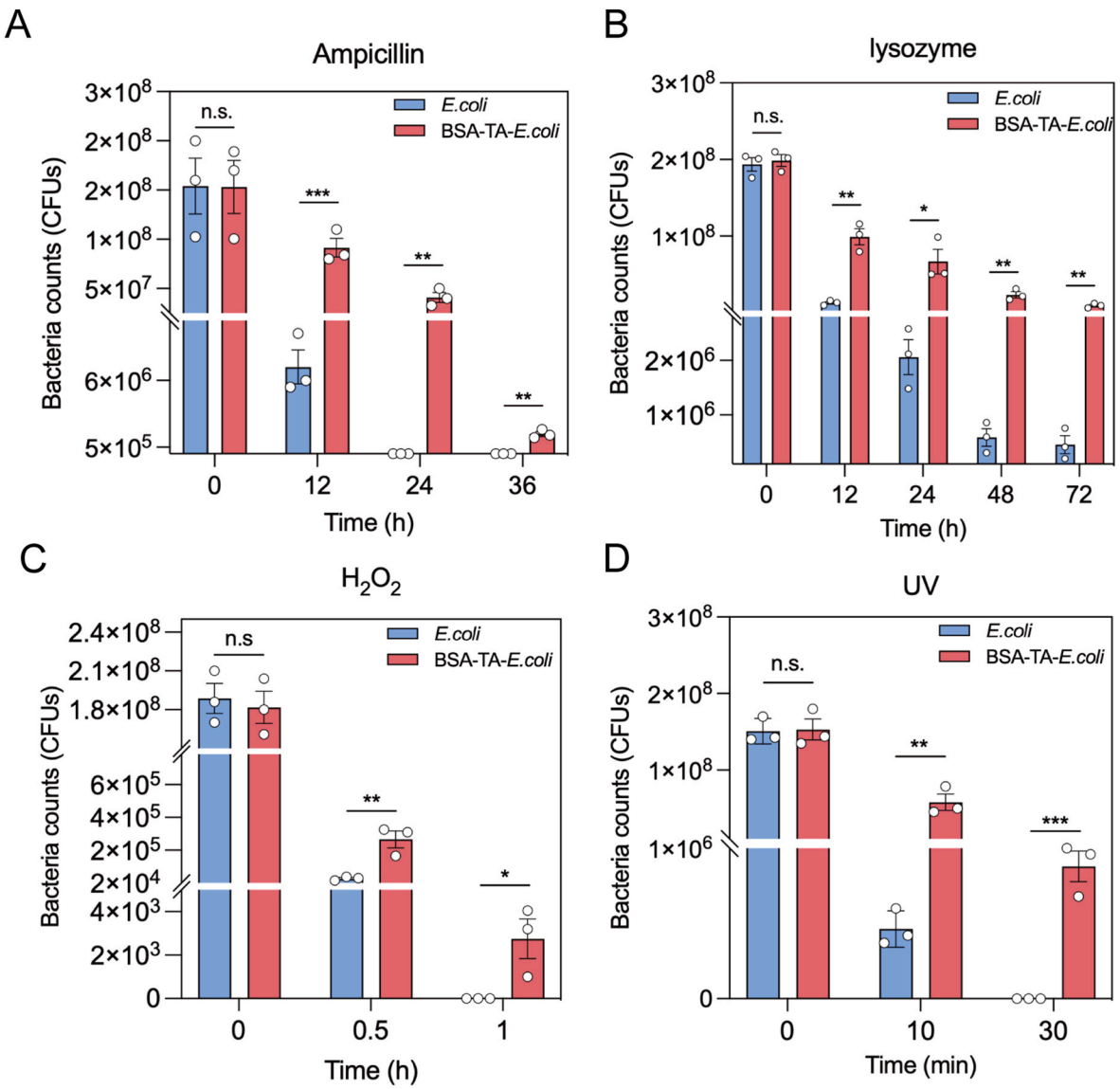

Fig. 3. Evaluation of BSA-TA-*E.coli* against environmental assaults. (**A-D**) Survival of *E.coli* and BSA-TA-*E.coli* after exposure to the following conditions: (**A**) LB medium with 0.25 mg/mL of Ampicillin, (**B**) LB medium with 20 mg/mL of Lysozyme, (**C**) LB medium with H_2O_2 (80 mM), (**D**) UV irradiation (254 nm). The number of surviving bacteria was quantified by spreading 50 μL of serially diluted samples onto LB agar plates and incubating at 37 °C for 24 h. CFU, colony-forming units. Data are presented as the mean ± SEM ($n = 3$). Statistical analysis was performed using Student's *t*-test. *$P < 0.05$, **$P < 0.01$, ***$P < 0.001$.

coating endowed bacteria with enhanced resistance against various environmental assaults.

3.3. Evaluation of stress responses of BSA-TA-E.coli in blood

To investigate the biocompatibility of BSA-TA-*E.coli* in blood, we measured the stress responses after bacteria treatment. Firstly, the in vitro hemolytic toxicity of BSA-TA-*E.coli* against murine erythrocytes was tested. As shown in Fig. 4A and Fig. S9, the uncoated *E.coli* showed severe hemolysis similar to that of triton X-100 (the positive control), whereas BSA-TA-*E.coli* displayed negligible hemolysis, suggesting that BSA-TA-*E.coli* is highly biocompatible. This might be attributed to the shielding effect of the BSA-TA coating, which keeps the bacteria from direct contact with blood and prevents the exposure and release of endotoxins. Next, the endotoxin levels induced by *E.coli* and BSA-TA-*E.coli* in vivo were measured via a chromogenic LAL endotoxin assay kit. According to the results in Fig. 4B, the endotoxin concentration in the BSA-TA-*E.coli* group was significantly lower than that of the *E.coli* group and maintained a low level during all detective timepoints. Notably, the endotoxin level was increased quickly after intravenous injection of *E. coli*, which might cause high-stress responses. However, it grew more slowly in the BSA-TA-*E.coli* group, indicating a good safety profile of BSA-TA-*E.coli*. Similar results were observed on another EcN bacteria, indicating the universality of the shielding effect of the BSA-TA coating on other bacteria (Fig. S10). Additionally, because *E.coli* is a pathogenic bacterium, all the mice died after intravenous injection for 2 days. In contrast, the BSA-TA layer encapsulated *E.coli* group showed a remarkably prolonged survival rate of mice, with over 66 % of the mice long-term surviving (Fig. 4C). Moreover, treatment with *E.coli* would cause damage to blood cells. Next, we evaluated the influence of *E.coli* and BSA-TA-*E.coli* on blood by measuring the complete blood counts after different bacteria injections. Compared with the negative control, the numbers of lymphocytes increased in the *E.coli* treatment group, while red blood cells, white blood cells, hemoglobin, and neutrocytes were dramatically reduced. However, the blood cells were unaffected by the BSA-TA-*E.coli* treatment, as evidenced by the comparable complete blood counts with healthy mice (Fig. 4D and Table S1). Furthermore, the levels of inflammatory cytokines in the blood, including IL-6, IL-10, IL-

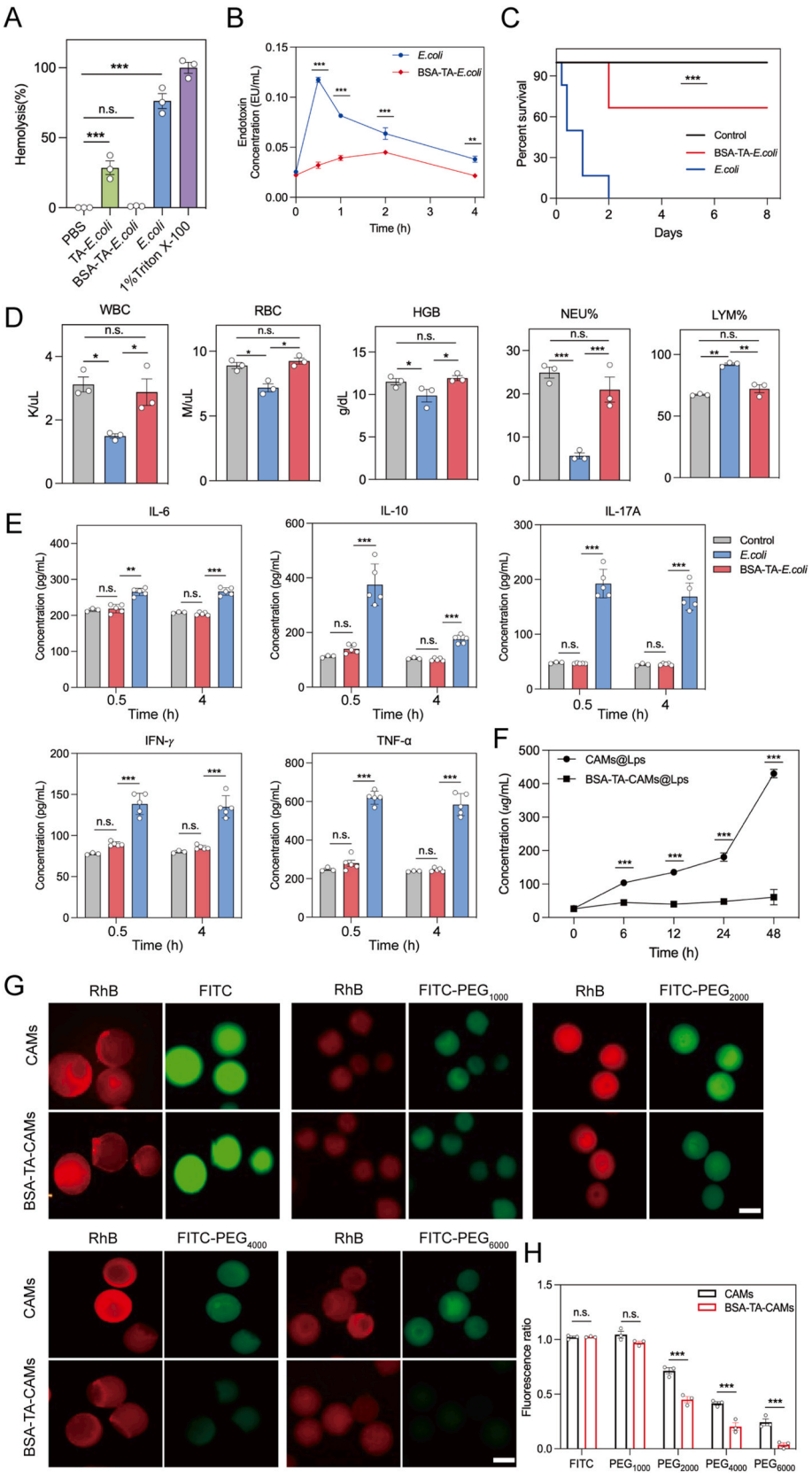

(caption on next page)

Fig. 4. Evaluation of stress responses of BSA-TA-*E.coli* on intravenous injection. (**A**) Hemolytic toxicity of *E.coli*, TA-*E.coli*, and BSA-TA-*E.coli* against murine erythrocytes. PBS served as the negative control, and Triton X-100 (1 %) served as the positive control. Data are presented as means ± SEM ($n = 3$). (**B**) Endotoxin level changes in mice after treatment with *E.coli* or BSA-TA-*E.coli* intravenously. Data are presented as means ± SEM ($n = 3$). (**C**) The survival rate of mice after intravenous injection of *E.coli* and BSA-TA-*E.coli* (1×10^7 CFUs). Data are presented as means ± SEM ($n = 6$). (**D**) Complete blood counts of mice after 30 min of intravenous injection of *E.coli* and BSA-TA-*E.coli*. PBS served as the negative control. RBC, red blood cell; WBC, white blood cell; HGB, hemoglobin; NEU, neutrocyte; LYM, lymphocyte. Data are presented as means ± SEM ($n = 3$). (**E**) Levels of cytokines in serum measured by ELISA kits, including IL-6, IL-10, IL-17A, TNF-α, and IFN-γ, after administration of *E.coli* and BSA-TA-*E.coli*, respectively. Data are presented as means ± SEM ($n = 5$). (**F**) The concentrations of released lipopolysaccharides (LPS) in the supernatant at different time points. LPS was first encapsulated in calcium alginate microspheres (CAMs@LPS) or BSA-TA-encapsulated CAMs, which were shaken at room temperature. The concentrations of LPS in the supernatant were detected to reflect the shielding effect of the BSA-TA coating against LPS release. (**G**) The permeability of different weight molecules to the BSA-TA layer. The calcium alginate microspheres (CAMs) or BSA-TA-encapsulated CAMs were co-incubated with different-weight FITC-labeled molecules in PBS for 6 h. The fluorescence in CAMs was imaged to evaluate the permeability of different-weight molecules. Scale bar, 100 mm. (**H**) The quantified fluorescence intensity ratio in CAMs. Data are presented as the mean ± SEM ($n = 3$ fields). Statistical analysis was performed using Student's *t*-test or one-way ANOVA. $^*P < 0.05$, $^{**}P < 0.01$, $^{***}P < 0.001$. (For interpretation of the references to color in this figure legend, the reader is referred to the Web version of this article.)

17A, TNF-α, and IFN-γ, were measured after intravenous injection of *E. coli* or BSA-TA-*E.coli* for 0.5 and 4 h. As shown in Fig. 4E, there was a substantial increase in cytokine levels in the uncoated *E.coli* treatment group. Nevertheless, all the tested cytokines in the BSA-TA-*E.coli* group had no significant differences compared to the negative control, indicating that the BSA-TA coating completely eliminated the stress responses caused by *E.coli*. Collectively, with the pathogenic strain of *E.coli* as the model bacterium, we proved that the BSA-TA coating remarkably

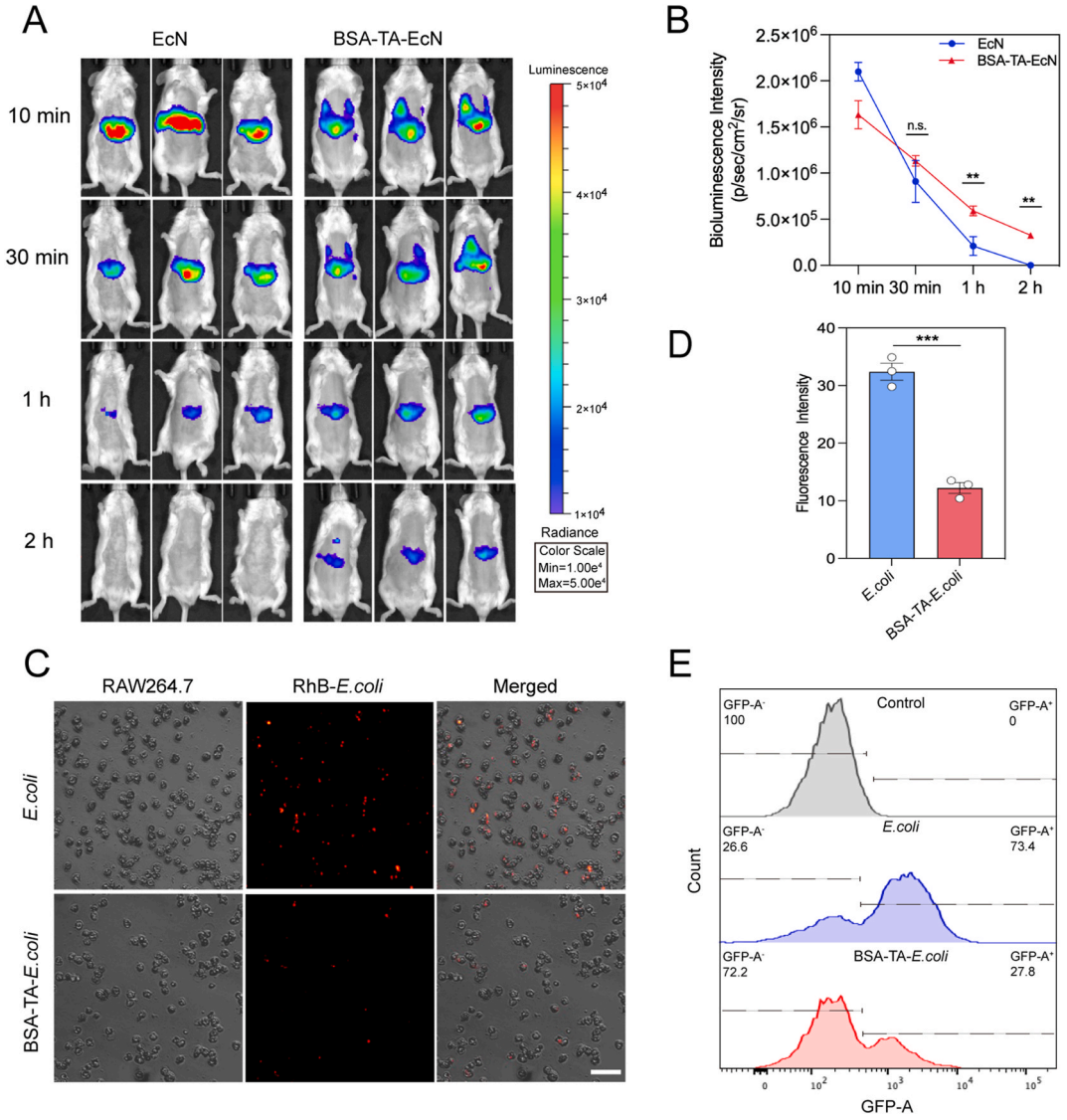

Fig. 5. Evaluation of the retention time of BSA-TA layer-encapsulated bacteria after intravenous injection. (**A**) Bioluminescence images of mice administered with bioluminescent bacteria formulations at different time points. (**B**) Bioluminescence decay curves of bioluminescence intensities of the mice at all pre-determined time points through Region-of-Interest analysis. (**C**) Representative fluorescence images of RAW 264.7 (mouse leukemia cells of monocyte-macrophage) after co-incubated with Rhodamine B-labeled *E.coli* or BSA-TA-*E.coli* for 1 h, and (**D**) Quantified fluorescence intensities through ImageJ software to reflect the engulfed bacteria by macrophages. Scale bar, 50 μm. (**E**) Quantitative analysis of RAW 264.7 that engulfs *E.coli* or BSA-TA-*E.coli* expressing GFP by flow cytometric analysis. Statistical analysis was performed using Student's *t*-test. $^*P < 0.05$, $^{**}P < 0.01$, $^{***}P < 0.001$, n.s., no significance.

enhanced the biocompatibility of bacteria without causing any stress responses, hence expanding the application of bacteria in vivo.

By taking into account the macromolecular profile of endotoxins, we established calcium alginate microspheres (CAMs) to resemble bacteria and investigated the ability of the BSA-TA layer to prevent the penetration of different weight molecules [31], thereby demonstrating its effectiveness in inhibiting the release of endotoxins from bacteria. The CAMs was prepared, and the BSA-TA layer was successfully encapsulated on the CAMs surface using a similar method (Fig. S11). Firstly, We chose LPS as one of the endotoxins and encapsulated it in CAMs or BSA-TA-encapsulated CAMs. At predetermined time points, the supernatant was taken, and the concentrations of LPS were measured via the phenol sulfuric acid method. As shown in Fig. 4F, the persistent release of LPS was observed in the CAMs@LPS, while there was almost no LPS released from BSA-TA-CAMs@LPS, indicating the preventing effect of the BSA-TA layer on the penetration of LPS. Moreover, to reflect the preventive effect of the BSA-TA layer on different weight molecules, we placed CAMs or BSA-TA-CAMs in solutions containing fluorescence-labeled different weight molecules and imaged the fluorescence in CAMs via a fluorescence microscope. As shown in Fig. 4G and H, for the small molecules, such as Rhodamine B, FITC, and FITC-PEG1000, the BSA-TA coating could hardly influence their diffusion, as evidenced by the similar fluorescence intensity between CAMs and BSA-TA-CAMs groups. Nevertheless, with an increase in molecular weight, the fluorescence intensity in BSA-TA-CAMs was dramatically reduced compared to that of CAMs, indicating that the BSA-TA coating impeded the penetration of larger molecules. Notably, the BSA-TA coating reduced the penetration of FITC-PEG6000 by 94.2 %. Overall, the BSA-TA layer functioned as a barrier that could block the penetration of macromolecules and had the capability to hinder the release of endotoxins by bacteria.

3.4. Preventable effects of the BSA-TA layer against bacterial clearance

Considering the shielding effect of the BSA-TA coating, we conducted further research on the duration of bacteria persistence after intravenous injection. Due to the significant mortality caused by the pathogenic bacterium of *E.coli* in mice, we selected EcN, a harmless bacterium with spontaneous bioluminescence, as a model to assess the duration of bacterial presence in vivo. After the injection of EcN and BSA-TA-EcN via the tail vein of mice, the bioluminescence intensity was monitored and imaged using an IVIS. As shown in Fig. 5A and B, the bioluminescence signals in the BSA-TA-EcN group decayed more slowly than that in the uncoated EcN group, suggesting that BSA-TA-EcN has a longer retention time in vivo. It is worth mentioning that the BSA-TA-EcN group maintained a significant bioluminescence signal after 2 h, but this signal disappeared in the EcN group (Fig. S12). The improved blood reservation might be attributed to the camouflage effect of the BSA-TA coating, which hindered the clearance of bacteria by phagocytes. To verify this hypothesis, we incubated *E.coli* and BSA-TA-*E.coli* with macrophages and analyzed them using fluorescence microscopy and flow cytometry. As anticipated, the engulfed BSA-TA-*E.coli* by macrophages were much less than those of the uncoated *E.coli*, as evidenced by the reduced fluorescence intensity of the rhodamine B-labeled bacteria (Fig. 5C and D). Moreover, the flow cytometry study revealed that 73.4 % of macrophages had *E.coli*, but only 27.8 % of macrophages contained BSA-TA-*E.coli* (Fig. 5E and Fig. S13). This indicates that the engulfment of bacteria after BSA-TA coating is reduced, and the results aligned well with the findings from fluorescence microscopy.

3.5. The reduced immunogenicity of bacteria resulting from the protected BSA-TA layer and the subsequent removal of the coating upon bacterial proliferation

The immunogenicity of bacteria would induce severe side effects and limit the applications of bacteria in vivo. To explore the protective effect of the BSA-TA coating to reduce the immunogenicity of bacteria, we chose the pathogenic strain of *E.coli*, encapsulated them with BSA-TA, and studied the stimulation effect on immune cells, including dendritic cells (DC2.4) and macrophages (RAW264.7), via a transwell assay. Specifically, the cells of *E.coli* or BSA-TA-*E.coli* were placed on the upper compartment of a 0.4 μm transwell chamber, which could prevent the penetration of bacteria. The DC2.4 or RAW264.7 cells in DMEM medium were inoculated in the lower compartment independently (Fig. 6A). After 12 h, the biomarker of MHC II that presents the maturation of DC cells was measured by flow cytometry, as well as the CD86 that stands for the M1 type of macrophages. As shown in Fig. 6B and C, the DC2.4 cells maturation rate of the BSA-TA-*E.coli* group was 37 %, while that was 93 % in the *E.coli* treatment, exhibiting a significantly reduced DC2.4 cells maturation rate in the BSA-TA-*E.coli* compared to the *E.coli*. Moreover, the results in macrophages showed that the BSA-TA-*E.coli* treatment induced lower macrophage polarization than the *E.coli* treatment (Fig. 6D and E). Collectively, the BSA-TA-*E.coli* showed reduced immunogenicity attributed to the shielding effect of the BSA-TA coating, as evidenced by the lowered DC2.4 cells maturation and macrophage polarization (Fig. 6F).

Subsequently, we investigated the stability of the BSA-TA coating on the bacterial surface. Following the encapsulation of the rhodamine B-labeled BSA-TA layer, the bacteria were immersed in PBS, kept at a temperature of 4 °C, and monitored the integrity of BSA-TA-*E.coli* at 12, 24, and 48 h by flow cytometry. The findings shown in Fig. 6G and **H** indicate that the BSA-TA layer was stable and remained adhered to the bacteria for the whole duration of the experiment. Furthermore, we conducted experiments to examine the detachment of the BSA-TA layer as a result of bacterial growth and proliferation. We placed the BSA-TA-*E.coli* in LB medium at 37 °C and evaluated the samples using flow cytometry and fluorescence microscopy at predetermined time points. After incubating for 1 h in this condition, the bacteria population increased by a factor of 1.6, then for 2, 4, 6, 8, and 12 h, it increased by a factor of 5.8, 72, 320, 1144, and 2202, respectively (Fig. S14). As the bacteria multiplied, the fluorescence intensity declined, indicating the BSA-TA layer's separation from the bacterial surface (Fig. 6I and S15). However, the decay rate of fluorescence intensity was significantly slower compared to the growth rate of bacteria, which might be contributing to the elasticity and adhesion of the TA layer. For instance, after 2 h, the fluorescence intensity was reduced by approximately 38 %, while the bacterial population was increased by 5.8 times. When the bacteria rose by 2202 times after 12 h, the fluorescence intensity almost completely disappeared (Fig. 6J). The delayed BSA-TA coating detachment would be advantageous for a delayed exposure of naked bacteria, therefore enhancing the biocompatibility of bacteria when applied to the body. The results were further confirmed by fluorescence microscopy. As shown in Fig. 6K, almost all the bacteria showed BSA-TA coating after 2 h, and the BSA-TA coating was completely removed after 12 h, which was consistent with the results of the flow cytometry analysis. Moreover, the stability and detachment of the BSA-TA coating were also evaluated in blood conditions, and the results were similar to those in the LB medium, as evidenced by the steady fluorescence at 4 °C and the gradual decrease in fluorescence at 37 °C (Fig. S16). Collectively, the BSA-TA coating is stable under bacterial resting circumstances, facilitating the storage and transportation of this bacterial formulation. Additionally, when bacteria grow and proliferate, the BSA-TA coating progressively detaches to release naked bacteria that might be favorable for bacteria-based imaging or therapeutic purposes. Notably, the detachment of the BSA-TA layer lasts for 12 h and is comparatively slower than bacterial growth, indicating a good safety profile of bacteria with BSA-TA coating.

3.6. In vivo tumor imaging and anti-tumor efficacy of BSA-TA-EcN

Furthermore, given the improved biocompatibility of bacteria after BSA-TA encapsulation, we explored the in vivo applications by

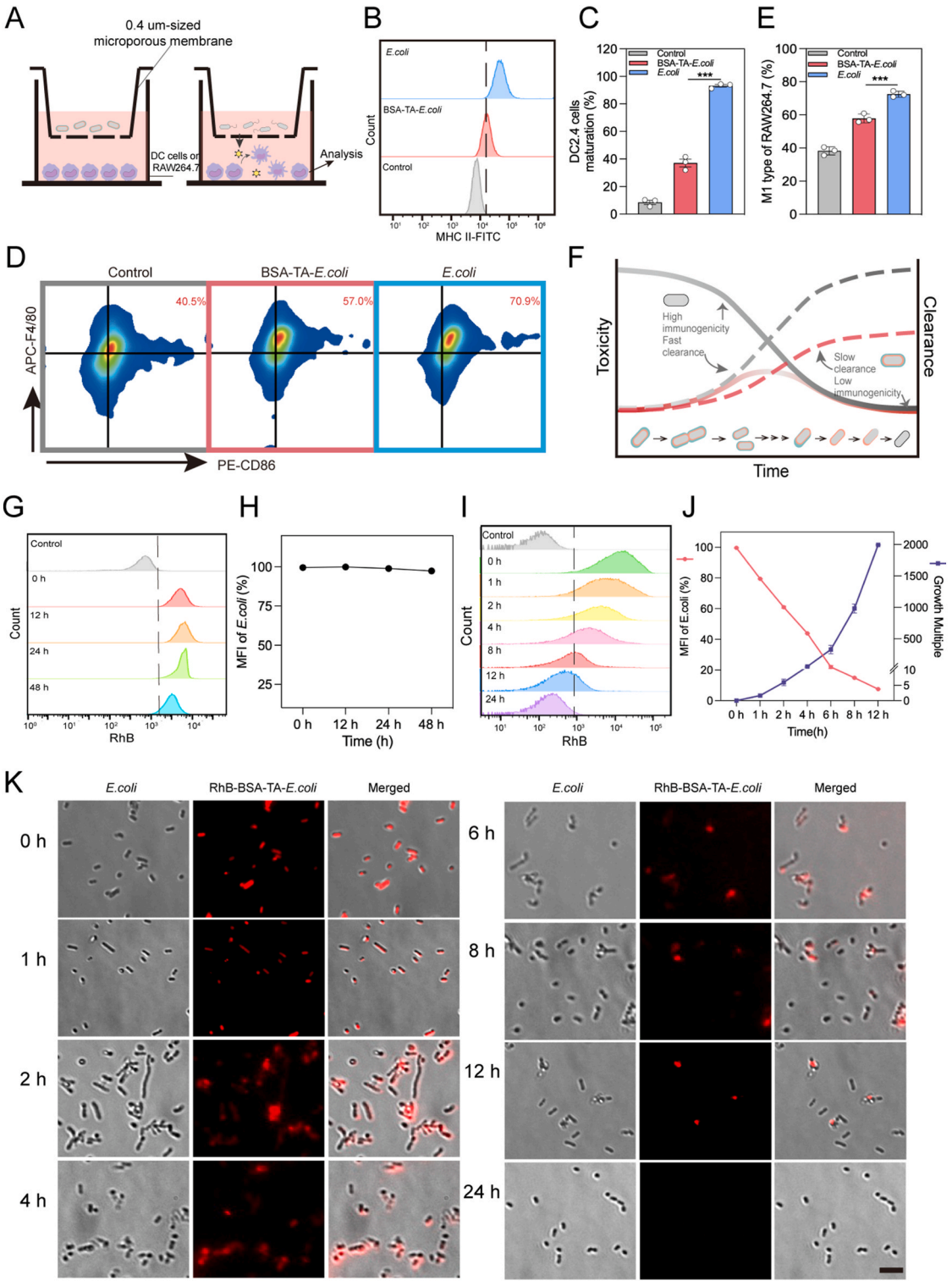

Fig. 6. Evaluation of the immunogenicity of the BSA-TA-coated bacteria and the process of detachment of the coating layer upon bacteria proliferation. (**A**) Schematic illustration to evaluate the immunogenicity of bacteria with or without BSA-TA coating via a transwell assay. The cells of *E.coli* or BSA-TA-*E.coli* in PBS were placed in the upper compartment of a 0.4-μm transwell chamber, while the lower compartment contained immune cells of RAW264.7 or DC2.4. The biomarkers in immune cells were detected by flow cytometry. (**B**) Flow cytometry assay of matured DC2.4 cells (MHC II ^{high}) and (**C**) quantified DC2.4 cell maturation after incubation with bacteria in the transwell chamber for 12 h (n = 3). (**D**) Representative flow cytometric plots and (**E**) quantitative analysis of M1 type macrophages (F4/80^{high} CD86^{high}) after indirect coculture with *E.coli* or BSA-TA-*E.coli* cells for 12 h (n = 3). (**F**) Schematic illustration of the BSA-TA layer's protective effect on bacteria. Owing to the protective effect of the BSA-TA layer, the bacteria displayed slower clearance and reduced immunogenicity compared to uncoated ones, exhibiting a good safety profile. (**G**) Flow cytometry analysis and (**H**) quantified ratios of Rhodamine B-labeled BSA-TA-*E.coli* after culturing in PBS at 4 °C. (**I**) Flow cytometry analysis of Rhodamine B-labeled BSA-TA-*E.coli* after incubation in LB medium at 37 °C for different times. No fluorescence labeled BSA-TA-*E.coli* served as the control. (**J**) The contrast between normalized mean fluorescence intensity (MFI) ratio of Rhodamine B-labeled BSA-TA-*E.coli* and bacterial multiplication fold after culturing in LB medium. Data are presented as means ± SEM (n = 3). (**K**) Representative fluorescent images of Rhodamine B-labeled BSA-TA-*E.coli* after incubation in LB medium at 37 °C for different times. Scale bar, 3 μm.

evaluating the tumor imaging and the therapeutic efficacy of BSA-TA-EcN against tumors. By establishing 4T1 tumor-bearing mice, 1×10^6 CFUs of EcN and BSA-TA-EcN with bioluminescence were injected, and the bioluminescence intensities of mice were monitored via an IVIS (Fig. 7A). As shown in Fig. 7B and C, strong bioluminescence signals were observed in mice and bacteria mainly appeared at the tumor sites after 3 days of bacteria injection, demonstrating the perfect tumor accumulation specificity. Moreover, the bacteria could maintain their bioluminescence in tumor tissues for multiple days, facilitating the long-term bioimaging of tumors. Notably, the bioluminescence intensity of the BSA-TA-EcN was significantly higher than EcN in all detective time points, and the bioluminescence signals of BSA-TA-EcN decayed slower than that of EcN. On day 7, all the mice injected with BSA-TA-EcN had strong bioluminescence signals in tumors, while that disappeared in most of the mice with EcN injection (Fig. 7D). The average bioluminescence intensity from isolated tumors in mice with BSA-TA-EcN injection was 5.4 times stronger than that of EcN at day 7 post-injection (Fig. 7E). Moreover, no bacteria were observed in other organs, further confirming the tumor-targeting specificity (Fig. 7F). Collectively, the BSA-TA-EcN showed excellent tumor-targeting capability and could maintain bioluminescence at the tumor site for over 7 days, indicating its potential as an effective tool for long-term tumor imaging.

Furthermore, we explored the anti-tumor efficacy of BSA-TA-EcN by establishing a 4T1 tumor-bearing mice model. After the tumor volume reached 80–120 mm^3, the mice were injected one dose with 1×10^7 CFUs of EcN or BSA-TA-EcN intravenously, and the tumor-bearing mice without bacteria administration served as the control. The body weight and tumor volume were monitored daily for 21 days (Fig. 7G). Due to the toxicity of EcN, all the mice injected with EcN died within six days. In contrast, 80 % of mice administered BSA-TA-EcN survived (Fig. 7H). Additionally, all the mice with bacteria injection showed weight loss in the first couple of days. Nevertheless, the weight loss in the BSA-TA-EcN group began to recover on day 3 and was completely restored after 13 days of bacteria injection, further demonstrating the remarkedly improved safety profiles upon the protection of the BSA-TA coating (Fig. 7I). Moreover, the BSA-TA-EcN significantly inhibited the growth of the tumors with only one dose administration. Conversely, the tumors in the control group grew quickly (Fig. 7J). After 21 days, the tumors were isolated and imaged. As shown in Fig. 7K, the tumors in the BSA-TA-EcN group were substantially smaller than the control. Specifically, the tumor weight in BSA-TA-EcN was 6.1 times lower than that in control, demonstrating the potent anti-tumor efficacy of BSA-TA-EcN (Fig. 7L). Overall, the BSA-TA coating endows bacteria with high safety profiles, and is able to broaden bacterial applications in tumor imaging and tumor therapy.

4. Discussion

Bacteria have favorable characteristics, such as diversity, genetic manipulation, surface modification, and tissue-targeting specificity, making them valuable in medical areas, like bioimaging, diagnosis, and bacteriotherapy [32,33]. However, their application in vivo is challenging due to the toxicities they hold, such as endotoxins, which can cause severe side effects on the body, like septicemia [34]. In this study, we developed a simple BSA-TA coating strategy on bacteria to significantly improve their biocompatibility for expanding their potential applications. With only 20 s to prepare, the TA layer can prevent macromolecules-including endotoxins from penetrating and does not influence the diffusion of small molecules. This impedes the release of endotoxins from bacteria but does not affect them ingesting essential nutrients for supporting their growth, exhibiting a remarkably reduced toxicity. Moreover, the adhesive capability of the TA layer enables the deposition of BSA by simple mixing [35]. The BSA originally present in blood gives bacteria high biocompatibility after encapsulation, which camouflages bacteria and prevents them from being phagocytized by phagocytes, thereby exhibiting a prolonged reservation in blood for enhanced potential applications. In addition, the BSA-TA coating shields the direct contact of bacteria with their surroundings, therefore avoiding any stress responses even administered via intravenous injection. Importantly, the BSA-TA coating does not affect the growth, proliferation, or motility characteristics of bacteria, preserving their inherent properties. Moreover, the protective effect of the BSA-TA coating on bacteria leads to a substantial increase in their resistance to various environmental challenges, such as antibiotics, lysozymes, oxidative stress, and UV radiation. This improved resistance is favorable for the storage and transportation of bacteria. Notably, the BSA-TA coating could separate in response to bacterial growth, releasing native bacteria and allowing the bacteria to exploit their own advantages. For example, after colonizing tumor tissues, the exposure of naked bacteria could cause immune responses to stimulate T cells for tumor therapy [36,37]. Besides, the rate of detachment is much slower than bacterial growth, which is helpful for specific tissue targeting before the BSA-TA coating falls off, showing a good safety profile. Furthermore, the BSA-TA coating strategy is universal for other cells, demonstrating the broad application of this coating method. We also evaluated the applications in tumor imaging and anti-tumor therapy using BSA-TA-EcN and demonstrated superior long-term tumor imaging and potent therapeutic efficacy against tumors with acceptable safety characteristics. Overall, the BSA-TA coating technique enhanced the biocompatibility of bacteria with living organisms and has the capacity to broaden the range of bacterial utilization in vivo for multiple purposes, including tumor imaging and anti-tumor therapy.

5. Conclusions

In summary, a double-layer coating technique using tannic acid (TA) and albumin (BSA) is developed for bacterial encapsulation, which camouflages bacteria to extend the reservation time in vivo and prevents endotoxin exposure and release, showing potent biocompatibility. Meanwhile, the inherent properties are retained. In mouse tumor models, the BSA-TA-coated bacteria showed significantly enhanced long-term tumor imaging and therapeutic efficacy against tumors. This technology offers the potential to expand the range of bacterial utilization in vivo for multiple purposes.

CRediT authorship contribution statement

Qing Guan: Writing – original draft, Project administration. **Junjie Chen:** Writing – review & editing, Project administration. **Zhaonan Liu:** Writing – review & editing, Formal analysis. **Jianfeng Xin:** Writing – review & editing. **Yu Chen:** Writing – review & editing. **Peng Wang:** Writing – review & editing, Supervision. **Jun Liu:** Writing – review & editing, Supervision, Funding acquisition, Conceptualization.

Ethics approval and consent to participate

All animal experimental procedures were conducted according to all relevant ethical regulations and strictly followed the protocols approved by the Institutional Animal Care and Use Committee at the Ocean University of China.

Consent for publication

This work has not been published previously and is not under consideration for publication elsewhere. Its publication is approved by all the authors and tacitly or explicitly by the responsible authorities where the work was carried out; if accepted, it will not be published elsewhere in the same form, in English or any other language, including electronically, without the written consent of the copyright holder.

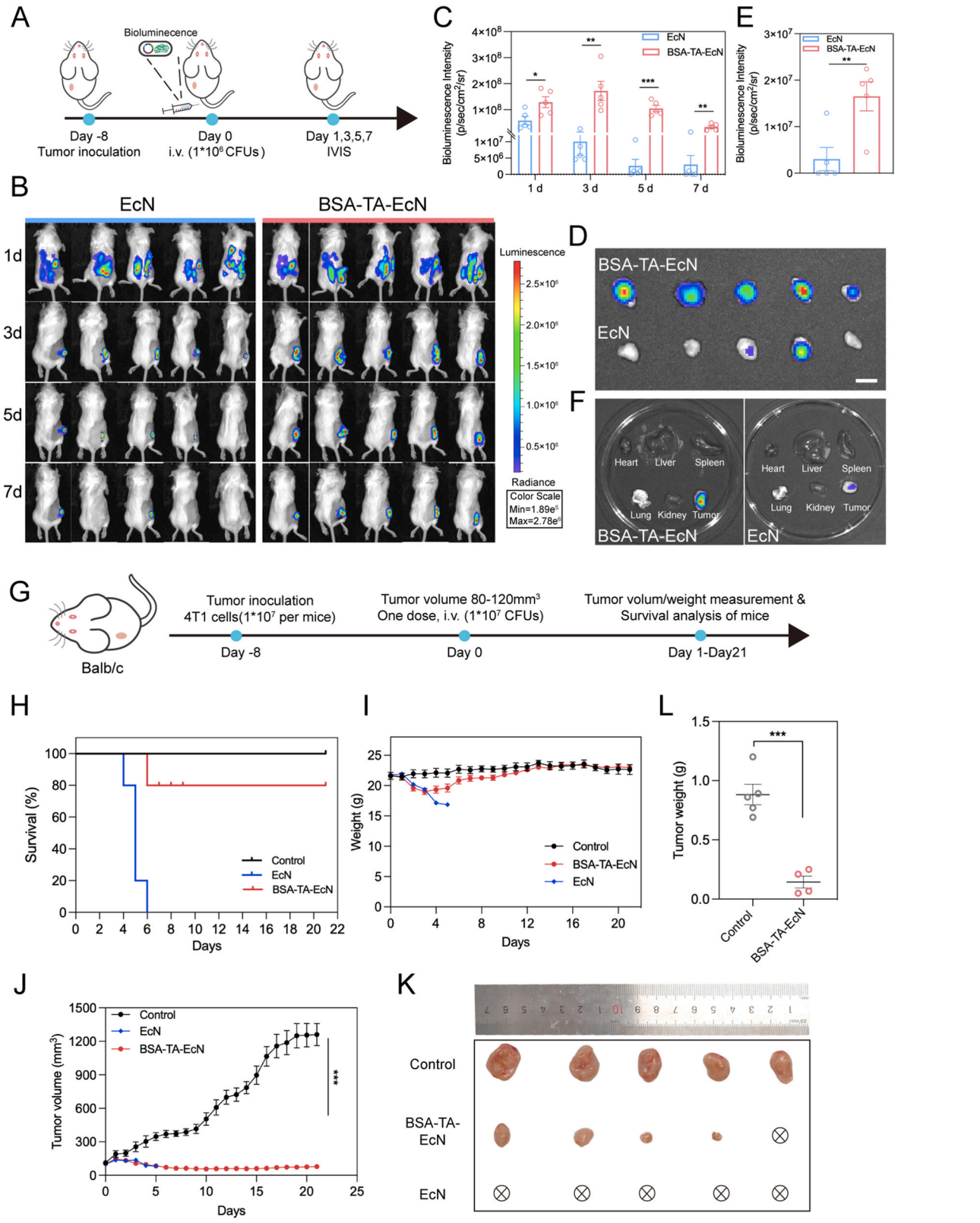

Fig. 7. In vivo tumor imaging and bacteriotherapy against tumors. (**A**) Schematic illustration for tumor imaging. (**B**) Tumor imaging of 4T1 tumor-bearing mice at 1, 3, 5, and 7 days post-injection of EcN or BSA-TA-EcN (1×10^6 CFUs) with bioluminescence. (**C**) Region-of-Interest analysis of bioluminescence intensities of the tumors. Error bars represent the standard deviation (n = 5). (**D**) Bioluminescence images of isolated tumors after 7 days of different bacteria administration. (**E**) Quantified bioluminescence intensities of tumors. (**F**) Representative bioluminescence images of major organs, including heart, liver, spleen, lung, kidney, and tumor, after 7 days post-administration of bacteria. (**G**) Schematic illustration of the bacterial safety assessment and the bacteriotherapy against tumor (n = 5). (**H**) Survival curves of the mice treated with different bacteria. The symbol ⊗ stands for mouse death. (**I**) Mouse body weight changes in 21 days after different bacteria treatments (1×10^7 CFUs) on 4T1 tumor-bearing mice. (**J**) Tumor growth curves after different treatments. The images of isolated tumors (**K**) and quantified tumor weight (**L**) after bacterial treatments on day 21. Significance was assessed using Student's *t*-test or one-way ANOVA. $^*P < 0.05$, $^{**}P < 0.01$, $^{***}P < 0.001$.

Funding

This work was supported by grants from the National Natural Science Foundations of China (Nos. 32370096 and 82003622), Natural Science Foundation of Shandong Province for Distinguished Young Scholars (Overseas, 2023HWYQ-068), Taishan Scholar Foundation of Shandong Province for Young Experts (tsqn202312092), and the start-up package from the Ocean University of China.

Declaration of competing interest

The authors declare that they have no known competing financial interests or personal relationships that could have appeared to influence the work reported in this paper.

Appendix A. Supplementary data

Supplementary data to this article can be found online at https://doi.org/10.1016/j.mtbio.2025.101788.

Data availability

Data will be made available on request.

References

[1] J. Liu, Y. Wang, W.J. Heelan, Y. Chen, Z. Li, Q. Hu, Mucoadhesive probiotic backpacks with ROS nanoscavengers enhance the bacteriotherapy for inflammatory bowel diseases, Sci. Adv. 8 (45) (2022) eabp8798.
[2] A. Fu, B. Yao, T. Dong, Y. Chen, J. Yao, Y. Liu, H. Li, H. Bai, X. Liu, Y. Zhang, Tumor-resident intracellular microbiota promotes metastatic colonization in breast cancer, Cell 185 (8) (2022) 1356–1372, e26.
[3] Z. Cao, S. Cheng, X. Wang, Y. Pang, J. Liu, Camouflaging bacteria by wrapping with cell membranes, Nat. Commun. 10 (1) (2019) 3452.
[4] D.-W. Zheng, P. Pan, K.-W. Chen, J.-X. Fan, C.-X. Li, H. Cheng, X.-Z. Zhang, An orally delivered microbial cocktail for the removal of nitrogenous metabolic waste in animal models of kidney failure, Nat. Biomed. Eng. 4 (9) (2020) 853–862.
[5] F. Cao, L. Jin, Y. Gao, Y. Ding, H. Wen, Z. Qian, C. Zhang, L. Hong, H. Yang, J. Zhang, Artificial-enzymes-armed Bifidobacterium longum probiotics for alleviating intestinal inflammation and microbiota dysbiosis, Nat. Nanotechnol. 18 (6) (2023) 617–627.
[6] L. Chen, J. Shen, Z. Kang, Z. Zhang, Z. Zheng, L. Zhang, Z. Xiao, Q. Zhang, H. Fang, J. Zhou, Fusobacterium nucleatum-mimicking nanovehicles to overcome chemoresistance for breast cancer treatment by eliminating tumor-colonizing bacteria, Chem. 10 (6) (2024) 1783–1803.
[7] N. Krishnan, L.J. Kubiatowicz, M. Holay, J. Zhou, R.H. Fang, L. Zhang, Bacterial membrane vesicles for vaccine applications, Adv. Drug Deliv. Rev. 185 (2022) 114294.
[8] J. Zhou, M. Li, Q. Chen, X. Li, L. Chen, Z. Dong, W. Zhu, Y. Yang, Z. Liu, Q. Chen, Programmable probiotics modulate inflammation and gut microbiota for inflammatory bowel disease treatment after effective oral delivery, Nat. Commun. 13 (1) (2022) 3432.
[9] L. Zhu, T. Yu, W. Wang, T. Xu, W. Geng, N. Li, X. Zan, Responsively degradable nanoarmor-assisted super resistance and stable colonization of probiotics for enhanced inflammation-targeted delivery, Adv. Mater. (2024) 2308728.
[10] C. Li, Z.X. Wang, H. Xiao, F.G. Wu, Intestinal delivery of probiotics: materials, strategies, and applications, Adv. Mater. (2024) 2310174.
[11] Z. Li, F. Mo, Y. Wang, W. Li, Y. Chen, J. Liu, T.-J. Chen-Mayfield, Q. Hu, Enhancing Gasdermin-induced tumor pyroptosis through preventing ESCRT-dependent cell membrane repair augments antitumor immune response, Nat. Commun. 13 (1) (2022) 6321.
[12] J. Li, X. Jiang, H. Li, M. Gelinsky, Z. Gu, Tailoring materials for modulation of macrophage fate, Adv. Mater. 33 (12) (2021) 2004172.
[13] J. Li, H. Zhou, C. Liu, S. Zhang, R. Du, Y. Deng, X. Zou, Biomembrane-inspired design of medical micro/nanorobots: from cytomembrane stealth cloaks to cellularized Trojan horses, Aggregate 4 (5) (2023) e359.
[14] C. Wang, L. Zhong, J. Xu, Q. Zhuang, F. Gong, X. Chen, H. Tao, C. Hu, F. Huang, N. Yang, Oncolytic mineralized bacteria as potent locally administered immunotherapeutics, Nat. Biomed. Eng. 8 (5) (2024) 561–578.
[15] V. Staedtke, N. Sun, R. Bai, Hypoxia-targeting bacteria in cancer therapy. Seminars in Cancer Biology, Elsevier, 2024.
[16] M. Chen, Q. Han, M. Zhang, Y. Liu, L. Wang, F. Yang, Q. Li, Z. Cao, C. Fan, J. Liu, Upconversion dual-photosensitizer–expressing bacteria for near-infrared monochromatically excitable synergistic phototherapy, Sci. Adv. 10 (10) (2024) eadk9485.
[17] X. Yi, H. Zhou, Y. Chao, S. Xiong, J. Zhong, Z. Chai, K. Yang, Z. Liu, Bacteria-triggered tumor-specific thrombosis to enable potent photothermal immunotherapy of cancer, Sci. Adv. 6 (33) (2020) eaba3546.
[18] J.-X. Fan, M.-T. Niu, Y.-T. Qin, Y.-X. Sun, X.-Z. Zhang, Progress of engineered bacteria for tumor therapy, Adv. Drug Deliv. Rev. 185 (2022) 114296.
[19] J. Ouyang, B. Deng, B. Zou, Y. Li, Q. Bu, Y. Tian, M. Chen, W. Chen, N. Kong, T. Chen, Oral hydrogel microbeads-mediated in situ synthesis of selenoproteins for regulating intestinal immunity and microbiota, J. Am. Chem. Soc. 145 (22) (2023) 12193–12205.
[20] M. Super, E.J. Doherty, M.J. Cartwright, B.T. Seiler, F. Langellotto, N. Dimitrakakis, D.A. White, A.G. Stafford, M. Karkada, A.R. Graveline, Biomaterial vaccines capturing pathogen-associated molecular patterns protect against bacterial infections and septic shock, Nat. Biomed. Eng. 6 (1) (2022) 8–18.
[21] A.C. Anselmo, K.J. McHugh, J. Webster, R. Langer, A. Jaklenec, Layer-by-Layer encapsulation of probiotics for delivery to the microbiome, Adv. Mater. 28 (43) (2016) 9486–9490.
[22] J. Liu, S. Yuan, A. Bremmer, Q. Hu, Convergence of nanotechnology and bacteriotherapy for biomedical applications, Adv. Sci. (2024) 2309295.
[23] E. Adriaenssens, B. Asselbergh, P. Rivera-Mejías, S. Bervoets, L. Vendredy, V. De Winter, K. Spaas, R. De Rycke, G. Van Isterdael, F. Impens, Small heat shock proteins operate as molecular chaperones in the mitochondrial intermembrane space, Nat. Cell Biol. 25 (3) (2023) 467–480.
[24] Y. Lyu, H. Huang, Y. Su, B. Ying, W.-C. Liu, K. Dong, N. Du, R.S. Langer, Z. Gu, K. Nan, Macroencapsulated bacteria for in vivo sensing and therapeutics, Matter 7 (4) (2024) 1440–1465.
[25] S.G. Ahmed, G. Oliva, M. Shao, X. Wang, J.J. Mekalanos, G.J. Brenner, Intratumoral injection of schwannoma with attenuated Salmonella typhimurium induces antitumor immunity and controls tumor growth, Proc. Natl. Acad. Sci. 119 (24) (2022) e2202719119.
[26] Y.C. Zeng, O.J. Young, C.M. Wintersinger, F.M. Anastassacos, J.I. MacDonald, G. Isinelli, M.O. Dellacherie, M. Sobral, H. Bai, A.R. Graveline, Fine tuning of CpG spatial distribution with DNA origami for improved cancer vaccination, Nat. Nanotechnol. (2024) 1–11.
[27] M. Musvosvi, H. Huang, C. Wang, Q. Xia, V. Rozot, A. Krishnan, P. Acs, A. Cheruku, G. Obermoser, A. Leslie, T cell receptor repertoires associated with control and disease progression following Mycobacterium tuberculosis infection, Nat. Med. 29 (1) (2023) 258–269.
[28] J. Liu, W. Li, Y. Wang, Y. Ding, A. Lee, Q. Hu, Biomaterials coating for on-demand bacteria delivery: selective release, adhesion, and detachment, Nano Today 41 (2021) 101291.
[29] H. Ejima, J.J. Richardson, K. Liang, J.P. Best, M.P. van Koeverden, G.K. Such, J. Cui, F. Caruso, One-step assembly of coordination complexes for versatile film and particle engineering, Science 341 (6142) (2013) 154–157.
[30] J. Stahl, B. König, A survey of the iron ligand-to-metal charge transfer chemistry in water, Green Chem. 26 (6) (2024) 3058–3071.
[31] T. Han, L. Chen, F. Gao, S. Wang, J. Li, G. Fan, H. Cong, B. Yu, Y. Shen, Preparation of thrombin-loaded calcium alginate microspheres with dual-mode imaging and study on their embolic properties in vivo, Eur. J. Pharm. Biopharm. 189 (2023) 98–108.
[32] L.-H. Peng, M.-Z. Wang, Y. Chu, L. Zhang, J. Niu, H.-T. Shao, T.-J. Yuan, Z.-H. Jiang, J.-Q. Gao, X.-H. Ning, Engineering bacterial outer membrane vesicles as transdermal nanoplatforms for photo-TRAIL–programmed therapy against melanoma, Sci. Adv. 6 (27) (2020) eaba2735.
[33] D.-H. Nguyen, A. Chong, Y. Hong, J.-J. Min, Bioengineering of bacteria for cancer immunotherapy, Nat. Commun. 14 (1) (2023) 3553.
[34] W. Li, Q. Liu, Y. Qian, C. Wang, C. Kong, L. Sun, L. Sun, H. Liu, Y. Zhang, D. Jiang, Adipose triglyceride lipase suppresses noncanonical inflammasome by hydrolyzing LPS, Nat. Chem. Biol. (2024) 1–9.
[35] S.J. Wu, X. Zhao, Bioadhesive technology platforms, Chem. Rev. 123 (24) (2023) 14084–14118.
[36] C.R. Gurbatri, N. Arpaia, T. Danino, Engineering bacteria as interactive cancer therapies, Science 378 (6622) (2022) 858–864.
[37] Z. Geng, Z. Cao, R. Liu, K. Liu, J. Liu, W. Tan, Aptamer-assisted tumor localization of bacteria for enhanced biotherapy, Nat. Commun. 12 (1) (2021) 6584.